Chemical bonding analysis for solid-state systems using intrinsic oriented quasiatomic minimal-basis-set orbitals

Y. X. Yao, C. Z. Wang, and K. M. Ho
Ames Laboratory–U.S. DOE and Department of Physics and Astronomy, Iowa State University, Ames, Iowa 50011, USA
(Received 30 March 2010; revised manuscript received 19 May 2010; published 16 June 2010)

A chemical bonding scheme is presented for the analysis of solid-state systems. The scheme is based on the intrinsic oriented quasiatomic minimal-basis-set orbitals (IO-QUAMBOs) previously developed by Ivanic and Ruedenberg for molecular systems. In the solid-state scheme, IO-QUAMBOs are generated by a unitary transformation of the quasiatomic orbitals located at each site of the system with the criteria of maximizing the sum of the fourth power of interatomic orbital bond order. Possible bonding and antibonding characters are indicated by the single particle matrix elements, and can be further examined by the projected density of states. We demonstrate the method by applications to graphene and (6,0) zigzag carbon nanotube. The oriented-orbital scheme automatically describes the system in terms of sp^2 hybridization. The effect of curvature on the electronic structure of the zigzag carbon nanotube is also manifested in the deformation of the intrinsic oriented orbitals as well as a breaking of symmetry leading to nonzero single particle density matrix elements. In an additional study, the analysis is performed on the Al_3V compound. The main covalent bonding characters are identified in a straightforward way without resorting to the symmetry analysis. Our method provides a general way for chemical bonding analysis of *ab initio* electronic structure calculations with any type of basis sets.

DOI: 10.1103/PhysRevB.81.235119 PACS number(s): 71.15.Ap, 71.20.−b, 73.61.Wp

I. INTRODUCTION

Density-functional theory (DFT) (Ref. 1) has been successfully applied to electronic structure and total energy calculations in solid-state systems for several decades. For many systems, the accuracy of the calculations can yield total energies that can be compared with experimental measurements and are relied on for predictions for complex structures ahead of experiments. However, in addition to numerical predictions, it would be desirable to have a deeper understanding of the nature of the chemical bonding in the systems.

Traditional atomic orbital-based chemical bonding analysis for molecules is usually based on a minimal basis description of the system, while results based on larger-size basis sets required for total energy convergence are usually not as intuitive. In previous work, Hoffmann showed that orbital-based chemical bonding analysis provides a qualitative understanding of the reaction of molecules on metal surfaces.[2] By extending Mulliken's bonding analysis for molecules to surface systems, Hoffmann introduced the crystal orbital overlap population (COOP) analysis.[3,4] However, the COOP analysis assumes that electronic structures are obtained with an implicit minimal-basis-set orbitals, as in extended Hückel type calculations.[2] Andersen developed a tight-binding (TB) approach with minimal-basis-set orbitals downfolded from the linear muffin-tin orbital (LMTO) method, which has been employed for COOP analysis.[5–7] Unfortunately, the exact downfolding scheme in the TB-LMTO method may not be generalizable to non-MTO electronic structure methods, e.g., the widely used pseudopotential (PP) method or projected augmented wave (PAW) method.[8–10] Some approaches, e.g., Sanchez's method based on projection of wave functions to optimized atomic orbital basis set, may be used for the COOP analysis in the general DFT calculations.[11] However, since the representation of the wave function by the atomic orbitals is not exact, some uncontrolled assumptions are involved in the process. In fact, a combination of PAW method and TB-LMTO method were used in the previous applications.[6,7] Therefore it is desirable to have an exact downfolding scheme which transforms the representation of the electronic structure from a large basis set (for example, plane waves) to a minimal atom-centered localized orbital basis set so that orbital-based bonding analysis like COOP can be directly applied.

Recently a scheme for generating an exact representation of the occupied electronic states of a system by quasiatomic minimal-basis-set orbitals (QUAMBO) has been developed.[12–15] The constructed QUAMBOs exhibit a maximal similarity to atomic orbitals and provide an excellent minimal basis set for chemical bonding analysis for molecular and solid-state systems. Mulliken charge and bond order analyses based on QUAMBOs have already been performed for crystalline solids.[12–15] We note that the maximally localized Wannier functions (MLWF) method may also provide an alternative approach for the exact downfolding of the electronic structures from general DFT calculations.[16] However, the objective of the MLWF approach is to achieve maximal localization by means of a unitary transformation of the Bloch wave functions, so the resultant WFs may not necessarily be centered on atoms,[16,17] hindering direct application to the COOP analysis.

Although the assignment of bond charge or bond order among atom pairs as performed in Refs. 12–15 is invariant with respect to the rotation of the orbitals at each atom, the orbital-resolved bonding analysis is dependent of the orientation of the orbitals.[5] Therefore intrinsic hybrid orbitals, e.g., sp^3 hybrids of carbon atom in diamond structure, would be a more appropriate choice for the basis set if we want more detailed orbital-resolved bonding information. Such hybrid orbital-based COOP analysis has been performed where the hybrid orbitals have to be constructed prior to the

bonding analysis by considering the local symmetry of the atoms in the crystal structures.[6,7] Nevertheless, an approach to obtain hybrid orbitals without resorting to local symmetry analysis is desired for general applications.[18] Ivanic and Ruedenberg recently proposed an automatic scheme based on QUAMBOs to get the intrinsic, oriented quasiatomic orbitals by unitary transformations on the orbitals for each atom in the molecule to maximize the sum of the fourth power of the interatomic orbital bond orders.[19] The method has been applied successfully to a number of molecular systems. In this paper, we generalize this intrinsic oriented QUAMBO scheme to solid-state systems and provide a general approach for chemical bonding analysis in solid-state systems by first-principles calculations.

The paper is organized as follows. Section II describes the detailed formalism for generating the IO-QUAMBOs. The applications of the method and discussions are given in Sec. III, followed by the summary and conclusion in Sec. IV.

II. METHOD

The detailed theoretical descriptions and technical discussions about how to generate highly localized QUAMBOs from first-principles wave functions can be found in Refs. 12–15. Hence here we only give a brief introduction to QUAMBO and aim to provide the formalisms on how to get the generalized intrinsic oriented QUAMBOs given the original unrotated QUAMBOs in periodic systems.

Let $\{\phi_\mu^{\mathbf{k}}\}$ be a set of band wave functions from DFT calculations on a solid-state system, a subset $C_o=\{\phi_\mu^{\mathbf{k}}|\mu=1,\ldots,N_o\}$ of which are to be exactly reproduced in the downfolded QUAMBO representation. $\mathbf{k}$ is the label for crystal momentum, and μ is the band index. In order to do that, one can choose N_Q QUAMBOs $\{\tilde{A}_{i\alpha}\}$ corresponding to a set of N_Q atomic orbitals $\{A_{i\alpha}\}$. Here i is the atomic site index and α is the orbital index (e.g., $s,p_x,p_y,p_z,\cdots$) in a unit cell. The angular momentum characters of the atomic orbitals can be determined by examining the site-projected angular momentum-resolved density of states. In general it is required that $N_Q \geq N_o$, i.e., the number of states preserved cannot be larger than the dimension of QUAMBOs. Another coherent set of Bloch wave functions, $C_{\bar{o}}=\{\phi_{\bar{\mu}}^{\mathbf{k}}|\bar{\mu}=1,\ldots,N_Q-N_o\}$, are constructed in the subspace orthogonal to the space spanned by C_o with the requirement of maximizing the similarity between the atomic orbitals and resultant QUAMBOs.[12–15] Then the Bloch sum of QUAMBO is obtained by a unitary transformation among the Bloch wave functions in set C_o and $C_{\bar{o}}$, i.e.,

$$|\tilde{A}_{i\alpha}^{\mathbf{k}}\rangle = f_{i\alpha}\left(\sum_{\mu=1}^{N_o}\langle\phi_\mu^{\mathbf{k}}|A_{i\alpha}^{\mathbf{k}}\rangle|\phi_\mu^{\mathbf{k}}\rangle + \sum_{\bar{\mu}=1}^{N_Q-N_o}\langle\phi_{\bar{\mu}}^{\mathbf{k}}|A_{i\alpha}^{\mathbf{k}}\rangle|\phi_{\bar{\mu}}^{\mathbf{k}}\rangle\right), \quad (1)$$

where $f_{i\alpha}$ is the normalization factor. The real space QUAMBO can be obtained by summation over momentum space,

$$|\tilde{A}_{i\alpha}^{n}\rangle = \frac{1}{\sqrt{N}}\sum_{\mathbf{k}} e^{-i\mathbf{k}\cdot\mathbf{R}_n}|\tilde{A}_{i\alpha}^{\mathbf{k}}\rangle. \quad (2)$$

Here $|A_{i\alpha}^n\rangle$ indicates QUAMBO $|A_{i\alpha}\rangle$ in nth unit cell with displacement vector $\mathbf{R}_n$. In real applications we find that QUAMBOs usually have some small deviations compared with the atomic orbitals which manifest effect of the local environment.

For the purpose of bonding analysis in the paper, QUAMBOs should be constructed such that the occupied and some unoccupied electronic states close to Fermi level (to capture low energy antibonding states) can be exactly reproduced in the representation of QUAMBOs. Mathematically, for a preserved band wave function $|\phi_\mu^{\mathbf{k}}\rangle$, it can always be exactly expressed in terms of the Bloch sums of the QUAMBOs, i.e.,

$$|\phi_\mu^{\mathbf{k}}\rangle = \sum_{i,\alpha} C_{i\alpha,\mu\mathbf{k}}|\tilde{A}_{i\alpha}^{\mathbf{k}}\rangle, \quad (3)$$

where $C_{i\alpha,\mu\mathbf{k}}$ is the coefficient.

The single particle density matrix $\hat{\rho}$ can then be expressed in terms of QUAMBOs

$$\begin{aligned}\hat{\rho} &= \sum_{\mu\mathbf{k}} f_{\mu\mathbf{k}}|\phi_\mu^{\mathbf{k}}\rangle\langle\phi_\mu^{\mathbf{k}}| \\ &= \frac{1}{N}\sum_{i\alpha n,j\beta m,\mu\mathbf{k}} f_{\mu\mathbf{k}}C_{j\beta,\mu\mathbf{k}}^* C_{i\alpha,\mu\mathbf{k}} e^{i\mathbf{k}\cdot(\mathbf{R}_n-\mathbf{R}_m)}|\tilde{A}_{i\alpha}^n\rangle\langle\tilde{A}_{j\beta}^m| \\ &= \sum_{i\alpha n,j\beta m}|\tilde{A}_{i\alpha}^n\rangle\pi_{in\alpha}^{jm\beta}\langle\tilde{A}_{j\beta}^m| \end{aligned} \quad (4)$$

with the density matrix element is defined as

$$\pi_{in\alpha}^{jm\beta} = \frac{1}{N}\sum_{\mu\mathbf{k}} f_{\mu\mathbf{k}}C_{j\beta,\mu\mathbf{k}}^* C_{i\alpha,\mu\mathbf{k}} e^{i\mathbf{k}\cdot(\mathbf{R}_n-\mathbf{R}_m)}, \quad (5)$$

where $f_{\mu\mathbf{k}}$ is the band occupation number. The off-diagonal element of the density matrix element, $\pi_{in\alpha}^{jm\beta}$ with $jm \neq in$, is referred to as a bond order between two orbitals on a pair of atoms.[19] Because of the translational symmetry in periodic systems, it is sufficient to consider the reduced single particle density matrix $\hat{\rho}_0$, i.e.,

$$\hat{\rho}_0 = \sum_{i\alpha,j\beta,m}|\tilde{A}_{i\alpha}^0\rangle\pi_{i0\alpha}^{jm\beta}\langle\tilde{A}_{j\beta}^m|. \quad (6)$$

Following Ivanic's approach,[19] the generalized intrinsic oriented QUAMBOs may be obtained by maximizing the hybridization-orientation sum (HOS)

$$\mathrm{HOS} = {\sum_{ia,jbm}}' \left(\sum_{\alpha\beta}\pi_{i0\alpha}^{jm\beta}D_{\alpha a}^{i0}D_{\beta b}^{jm}\right)^4 \quad (7)$$

with a series of orthogonal transformations (D) among the orbitals centered on each atom in the unit cell under the constraint of translational symmetry between $|\tilde{A}_{i\alpha}^m\rangle$ and $|\tilde{A}_{i\alpha}^n\rangle$. Σ' in Eq. (7) implies $i \neq j$ when $m=0$, so that the intra-atom contributions are excluded. D^{jm} is an orthogonal transformation matrix for the orbitals at jth atom in mth unit cell.

The maximization of HOS can be achieved by two steps. The first step is to perform a singular value decomposition of the following $N_{Qi}\times(N_Q\times N-N_{Qi})$ rectangular matrix (π_{i0}) for each atom i in the unit cell

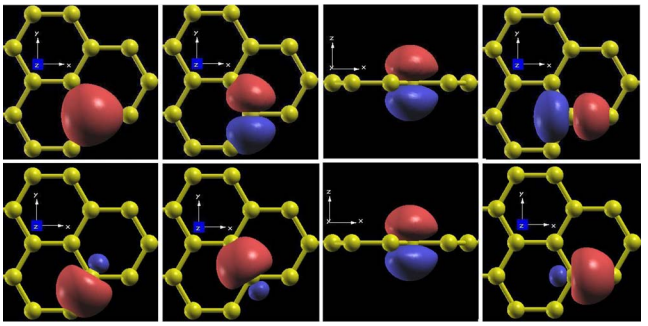

FIG. 1. (Color online) Upper panel: 3D contour plot of the original unrotated s-, p_y-, p_z-, p_x-like QUAMBOs for a carbon atom in graphene. Lower panel: Oriented QUAMBOs for a carbon atom in graphene with sp^2 hybridization.

$$\pi_{i0} = [\pi_{i0}^{\bar{i}_1 0} \pi_{i0}^{\bar{i}_2 0} \cdots \pi_{i0}^{i_1 1} \pi_{i0}^{i_2 1} \cdots] \tag{8}$$

where $\bar{i}$ runs over all the atoms in the unit cell except the ith atom. N_{Qi} is the total number of QUAMBOs associated with atom i. π_{i0}^{jm} is a $N_{Qi} \times N_{Qj}$ submatrix with elements $\pi_{i0\alpha}^{jm\beta}$. N is the number of nearest neighbor unit cells taken into consideration. The orthogonal matrix ($\mathbf{U}_{i0}$) composed of the left singular vectors of matrix π_{i0} can serve as a first try of rotating the orbitals on atom i to maximize HOS. By translational symmetry, $\mathbf{U}_{in}$ is same as $\mathbf{U}_{i0}$. With the transformation of $\mathbf{U}_{in}$, the rotated orbitals would be

$$|\tilde{A}_{i\alpha'}^{n}\rangle = \sum_{\alpha} |\tilde{A}_{i\alpha}^{n}\rangle \mathbf{U}_{in}(\alpha, \alpha') \tag{9}$$

and the density matrix becomes

$$\tilde{\pi}_{i0}^{jm} = (\mathbf{U}_{i0})^{\dagger} \pi_{i0}^{jm} (\mathbf{U}_{jm}). \tag{10}$$

The maximization of HOS is further achieved by a series of 2×2 Jacobi rotations (J) between the every pair of orbitals on each atom iteratively. Considering an initial pair of orbitals $|\tilde{A}_{i\alpha_1}^{0}\rangle$ and $|\tilde{A}_{i\alpha_2}^{0}\rangle$, the resultant orbitals under the Jacobi rotation would be

$$|\tilde{A}_{i\alpha_1}^{\prime 0}\rangle = |\tilde{A}_{i\alpha_1}^{0}\rangle J_{11} + |\tilde{A}_{i\alpha_2}^{0}\rangle J_{21},$$

$$|\tilde{A}_{i\alpha_2}^{\prime 0}\rangle = |\tilde{A}_{i\alpha_1}^{0}\rangle J_{12} + |\tilde{A}_{i\alpha_2}^{0}\rangle J_{22} \tag{11}$$

with

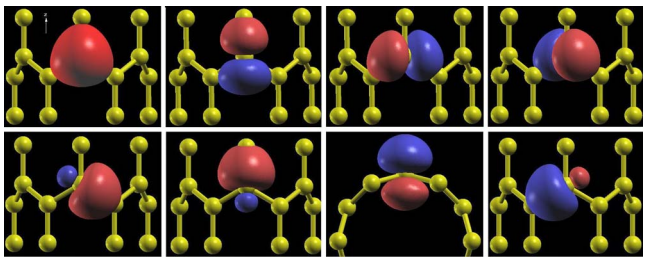

FIG. 2. (Color online) Upper panel: 3D contour plot of the original unrotated s-, p_y-, p_z-, p_x-like QUAMBOs for a carbon atom in zigzag SWCT (6,0). Lower panel: Oriented QUAMBOs for a carbon atom in zigzag SWCT (6,0) with sp^2-type hybridization.

$$J = \begin{pmatrix} \cos\gamma & -\sin\gamma \\ \sin\gamma & \cos\gamma \end{pmatrix}. \tag{12}$$

By translational symmetry, $|\tilde{A}_{i\alpha_1}^{n}\rangle$ and $|\tilde{A}_{i\alpha_2}^{n}\rangle$ would undergo the same rotation. Let the initial and resultant density matrix element be $\pi_{i0\alpha}^{jm\beta}$ and $\tilde{\pi}_{i0\alpha}^{jm\beta}$. The relevant part of HOS which will change accordingly is

$$\begin{aligned} \mathrm{HOS}^{*} &= \sum_{j,m,v\beta}{}' ((\tilde{\pi}_{i0a_v}^{jm\beta})^4 + (\tilde{\pi}_{i0\beta}^{jma_v})^4) + \sum_{m\neq 0, vv'} (\tilde{\pi}_{i0a_v}^{ima_{v'}})^4 \\ &= \sum_{j,m,v\beta}{}' \left(\sum_{k} \pi_{i0\alpha_k}^{jm\beta} J_{kv} + \sum_{k} \pi_{i0\beta}^{jm\alpha_v} J_{kv} \right)^4 \\ &\quad + \sum_{m\neq 0, vv'} \left(\sum_{kk'} \pi_{i0\alpha_k}^{im\alpha_{k'}} J_{kv} J_{k'v'} \right)^4 = \sum_{klpq} (P_{klpq} \\ &\quad + P^{klpq}) J_{klpq} + \sum_{klpq,k'l'p'q'} P_{klpq}^{k'l'p'q'} J_{klpq} J_{k'l'p'q'} \end{aligned} \tag{13}$$

Σ' implies $j \neq i$ if $m=0$ and $\beta \neq a_v$ if $j=i$. $v,k,l,p,q,v',k',l',p'q'=1,2$. The definitions of the shorthand notations are

$$P_{klpq} = \sum_{j,m,\beta}{}' \pi_{i0\alpha_k}^{jm\beta} \pi_{i0\alpha_l}^{jm\beta} \pi_{i0\alpha_p}^{jm\beta} \pi_{i0\alpha_q}^{jm\beta}, \tag{14}$$

$$P^{klpq} = \sum_{j,m,\beta}{}' \pi_{i0\beta}^{jm\alpha_k} \pi_{i0\beta}^{jm\alpha_l} \pi_{i0\beta}^{jm\alpha_p} \pi_{i0\beta}^{jm\alpha_q}, \tag{15}$$

$$J_{klpq} = \sum_{v} J_{kv} J_{lv} J_{pv} J_{qv} \tag{16}$$

and

TABLE I. A block of the single particle density matrix associated with a pair of nearest neighbor atoms in graphene. Left half is in the original unrotated QUAMBO representation, and the right half is for the oriented QUAMBOs.

	s	p_y	p_z	p_y		$(sp^2)_I$	$(sp^2)_{II}$	p_z	$(sp^2)_{III}$
s	0.05	**−0.12**	0.00	−0.07	$(sp^2)_I$	**0.36**	−0.05	0.00	−0.05
p_y	**0.12**	**−0.24**	0.00	**−0.12**	$(sp^2)_{II}$	0.05	−0.01	0.00	0.01
p_z	0.00	0.00	**0.17**	0.00	p_z	0.00	0.00	**0.17**	0.00
p_x	0.07	**−0.12**	0.00	**−0.10**	$(sp^2)_{III}$	0.05	0.01	0.00	−0.01

TABLE II. A block of the single particle density matrix associated with a pair of nearest neighbor atoms in SWCN (6,0). Left half is in the original unrotated QUAMBO representation, and the right half is for the oriented QUAMBOs.

π_{10}^{20}	s	p_y	p_z	p_y	$\tilde{\pi}_{10}^{20}$	$(sp^2)_I$	$(sp^2)_{II}$	p_z	$(sp^2)_{III}$
s	0.05	−0.07	0.01	**0.13**	$(sp^2)_I$	−0.01	0.05	−0.02	−0.01
p_y	0.07	**−0.10**	0.00	**0.13**	$(sp^2)_{II}$	−0.05	**0.35**	0.00	0.05
p_z	0.08	−0.06	**0.13**	**0.10**	p_z	*0.02*	0.00	**0.16**	0.00
p_x	**−0.10**	**0.11**	0.09	**−0.20**	$(sp^2)_{III}$	−0.01	−0.05	0.00	0.00

$$P_{klpq}^{k'l'p'q'} = \sum_{m\neq 0} \pi_{i0\alpha_k}^{im\alpha_{k'}} \pi_{i0\alpha_l}^{im\alpha_{l'}} \pi_{i0\alpha_p}^{im\alpha_{p'}} \pi_{i0\alpha_q}^{im\alpha_{q'}}. \tag{17}$$

Because of the symmetry with index permutation in p_{klpq}, J_{klpq} and $p_{klpq}^{k'l'p'q'}$, HOS* can be reduced to

$$\mathrm{HOS}^* = P_0 + P_{c1}\cos 4\gamma + P_{c2}\cos 8\gamma + P_{s1}\sin 4\gamma + P_{c2}\sin 8\gamma \tag{18}$$

with the abbreviated notations defined as

$$\begin{aligned} P_0 = \frac{1}{32}(&24(P_{1111}+P^{1111}) + 19P_{1111}^{1111} + 30P_{1111}^{1122} + 19P_{1111}^{2222} \\ &+ 4P_{1112}^{1112} + 12P_{1112}^{1121} - 12P_{1112}^{1222} - 4P_{1112}^{2221} \\ &+ 48(P_{1122}+P^{1122}) + 30P_{1122}^{1111} + 18P_{1122}^{1122} + 72P_{1122}^{1221} \\ &+ 18P_{1122}^{2211} + 30P_{1122}^{2222} - 12P_{1222}^{1112} + 4P_{1222}^{1222} + 12P_{1222}^{2221} \\ &- 4P_{2221}^{1112} + 24(P_{2222}+P^{2222}) + 19P_{2222}^{1111} + 30P_{2222}^{1122} \\ &+ 19P_{2222}^{2222}), \end{aligned} \tag{19}$$

$$\begin{aligned} P_{c1} = \frac{1}{8}(&2(P_{1111}+P^{1111}) + 3P_{1111}^{1111} - 6P_{1111}^{1122} + 3P_{1111}^{2222} \\ &- 12(P_{1122}+P^{1122}) - 6P_{1122}^{1111} - 6P_{1122}^{1122} - 24P_{1122}^{1221} \\ &- 6P_{1122}^{2211} - 6P_{1122}^{2222} + 2(P_{2222}+P^{2222}) + 3P_{2222}^{1111} - 6P_{2222}^{1122} \\ &+ 3P_{2222}^{2222}) \end{aligned} \tag{20}$$

$$\begin{aligned} P_{c2} = \frac{1}{32}(&P_{1111}^{1111} - 6P_{1111}^{1122} + P_{1111}^{2222} - 4P_{1112}^{1112} - 12P_{1112}^{1121} + 12P_{1112}^{1222} \\ &+ 4P_{1112}^{2221} - 6P_{1122}^{1111} + 6P_{1122}^{1122} + 24P_{1122}^{1221} + 6P_{1122}^{2211} - 6P_{1122}^{2222} \\ &+ 12P_{1222}^{1112} - 4P_{1222}^{1222} - 12P_{1222}^{2221} + 4P_{2221}^{1112} + P_{2222}^{1111} - 6P_{2222}^{1122} \\ &+ P_{2222}^{2222}), \end{aligned} \tag{21}$$

$$\begin{aligned} P_{s1} = \frac{1}{4}[&3P_{1111}^{1112} - 3P_{1111}^{1222} + 4(P_{1112}+P^{1112}) + 3P_{1112}^{1111} + 3P_{1112}^{1122} \\ &+ 3P_{1112}^{1221} + 3P_{1112}^{2222} + 3P_{1122}^{1112} - 3P_{1122}^{1222} - 3P_{1122}^{2221} + 3P_{1221}^{1112} \\ &- 4(P_{1222}+P^{1222}) - 3(P_{1222}^{1111} + P_{1222}^{1122} + P_{1222}^{2222} + P_{2221}^{1122} \\ &- P_{2222}^{1112} + P_{2222}^{1222})], \end{aligned} \tag{22}$$

and

$$\begin{aligned} P_{s2} = \frac{1}{8}(&P_{1111}^{1112} - P_{1111}^{1222} + P_{1112}^{1111} - 3P_{1112}^{1122} - 3P_{1112}^{1221} + P_{1112}^{2222} \\ &- 3P_{1122}^{1112} + 3P_{1122}^{1222} + 3P_{1122}^{2221} - 3P_{1221}^{1112} - P_{1222}^{1111} + 3P_{1222}^{1122} \\ &- P_{1222}^{2222} + 3P_{2221}^{1122} + P_{2222}^{1112} - P_{2222}^{1222}) \end{aligned} \tag{23}$$

Since HOS* is a periodic function of γ in the range of $[-\frac{\pi}{8}, \frac{\pi}{8})$, it is very easy to numerically locate the optimum γ^* which maximizes HOS*. In practice, several cycles of these consecutive Jacobi rotations are necessary to reach the maximum of HOS.

III. RESULTS

The generalized IO-QUAMBO generation scheme was applied to graphene system where the sp^2 hybridization for carbon atom is well established. The upper panel in Fig. 1 shows the unrotated s-, p_y-, p_z-, p_x-like QUAMBOs centered on a carbon atom in graphene. The resultant oriented QUAMBOs are plotted in the lower panel. One can see that our scheme automatically produces the sp^2 hybridization while the p_z-like QUAMBO remains unaffected.

The single particle density matrix elements associated with a pair of nearest neighbor atoms in the representation of original and oriented QUAMBOs are listed in Table I, where the left(right) are obtained before(after) the orbital rotation. The significant entries with a value larger than 0.10 are highlighted. It is clear that the number of the significant entries of the matrix in terms of oriented QUAMBOs is much reduced relative to the original one, which confirms that the density matrix is greatly simplified in the representation of the oriented QUAMBOs. The bond order between p_z-like and non-p_z-like orbitals is zero, indicating that p_z-derived bands (π, π^* bands) are decoupled from the non-p_z-derived bands, which is a result of the D_6 symmetry.

While the ideal sp^2 hybrid orbitals exist in the highly symmetric graphene system, physically the hybrid orbitals should not be very sensitive to the local symmetry. When a system is distorted in some reasonable range, the hybrid orbitals are expected to remain with some deformations which manifest the effect of the structural deviation from the local symmetry on the electronic structure. A good example for this testing case is the single wall carbon nanotube (SWCN) with small radius. We applied our method to zigzag SWCT (6,0) where the curvature effect on the electronic structure has been well established.[20] The lower panel of Fig. 2 shows the 3D contour plot of the IO-QUAMBOs for a carbon atom in the SWCT. The original unrotated QUAMBOs are also

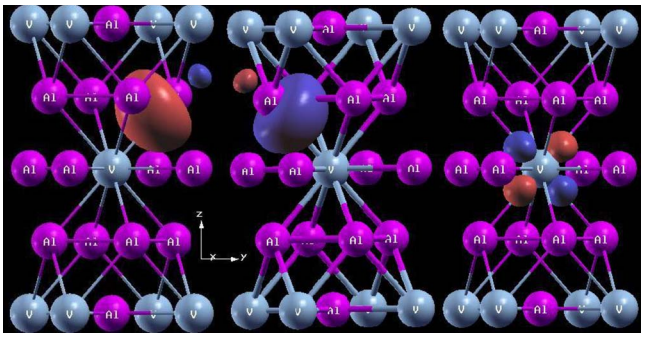

FIG. 3. (Color online) sp^3 hybrid orbitals of two Al atoms in the pure Al layer (left two) and d_{yz} orbital of V atom (right one). The four sp^3 hybrid orbitals (other two symmetric ones not shown) and one d_{yz} orbital will form bonding and antibonding states.

shown in the upper panel of Fig. 2 for comparison. The curvature of the geometry results in the asymmetric lobes of the third orbital which corresponds to the p_z-like orbital in the graphene. The other three orbitals remain clear sp^2-type hybridization similar to that in graphene. The misorientation of the original orbitals comes from the fact that the nearest neighbors of the atom are not exactly located in the axis plane generally. The physically reasonable orientation and hybridization of the orbitals are automatically obtained by our generalized orbital rotation scheme.

The curvature effect can be further studied by examining the single particle density matrix, a block of which is listed in Table II for a pair of nearest neighbor atoms. One can see that the bond order between p_z-like orbital and some non-p_z-like orbital is not zero as shown by the slanted matrix elements. As a result, p_z-derived bands (π, π^* bands) and the non-p_z-derived bands become coupled.

To further show that our method for chemical bonding analysis performs well even for complex structures, we applied it to Al_3V system, where a combination of PAW method and TB-LMTO method and sophisticated point group symmetry analysis have been used to reveal the covalent bonding nature.[6] Our orbital orientation scheme automatically generates the sp^3 hybridization of Al atom in the pure Al layers as shown in Fig. 3. Single particle density matrix also shows that the bond order between the V-d_{yz} orbital and the adjacent Al-sp^3 hybrid orbital is dominant. Thus V-d_{yz} orbital and the four nearest Al-sp^3 hybrid orbitals are expected to form bonding and antibonding states. Figure 4 shows the differential projected density of states (PDOS) on bonding and antibonding combinations of the automatically generated V-d_{yz} and Al-sp^3 orbitals in panel C. Such defined PDOS is equivalent to the differential COOP by Hoffmann.[6] The bonding state is dominant below Fermi-level, while the antibonding state turns to be the major contribution above the Fermi-level in the PDOS. Hence it shows unambiguously a bonding-antibonding characteristics between these orbitals, in agreement with Ref. 6. Figure 4 shows that the QUAMBO-based tight-binding approach reproduces the density of states from DFT calculations up to 4 eV above Fermi level in panel A, which justifies the employment of QUAMBOs to perform bonding-antibonding analysis. The PDOS on V-d_{yz} and Al-sp^3 are also shown in panel B of Fig. 3 for reference. A pseudogap around Fermi level in both PDOS might be an indication of covalent bonding characteristics. We have also examined the other symmetrically inequivalent oriented orbitals and found that they generally do not have a clear hybridization form. The corresponding single particle density matrix does not exhibit any clear dominant bonding either. This implies that the shape of the intrinsic oriented-orbital already conveys some information on the chemical bonding nature.

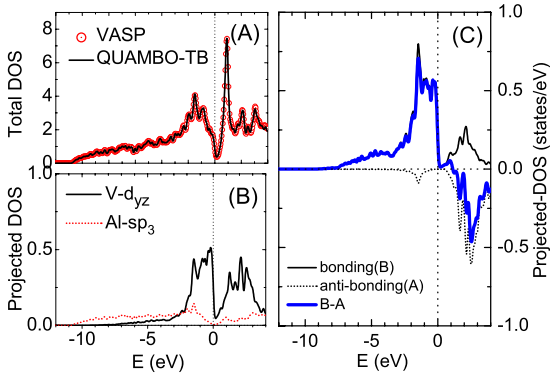

FIG. 4. (Color online) (a) Comparison between the total density of states obtained from DFT (circle) and that from *ab initio* QUAMBO-based tight-binding approach (line). (b) Density of states projected on d_{yz} orbital of V atom (straight line) and one sp_3 hybrid orbital of Al atom in the pure Al layer (dotted line). (c) Density of states projected on the bonding (thin straight line) and antibonding (thin dotted line) combinations of orbitals and their difference (thick line).

IV. CONCLUSION

A generalized orbital rotation scheme based on maximizing the sum of the interatomic orbital bond orders has been developed. The usefulness and generality of the scheme for chemical bonding analysis in solid-state systems has been illustrated by applications to graphene, carbon nanotube and Al_3V systems. The hybrid orbitals can be automatically generated without using local symmetry analysis, and the chemical bonding nature can also be identified by examining the single particle density matrix and projected density of states thereafter. Since QUAMBOs can be obtained in the Bloch space within a projection-based approach, our method provides a general basis-independent way to perform chemical bonding analysis for *ab initio* electronic structure calculations.

ACKNOWLEDGMENTS

Work at the Ames laboratory was supported by the U.S. Department of Energy, Office of Basic Energy Science, including a grant of computer time at the National Energy Research Supercomputing Center (NERSC) at the Lawrence Berkeley National Laboratory under Contract No. DE-AC02-07CH11358.

[1] P. Hohenberg and W. Kohn, Phys. Rev. **136**, B864 (1964); W. Kohn and L. J. Sham, *ibid.* **140**, A1133 (1965).
[2] R. Hoffmann, J. Phys.: Condens. Matter **5**, A1 (1993).
[3] R. Hoffmann, Rev. Mod. Phys. **60**, 601 (1988).
[4] R. Hoffmann, *Solids and Surfaces—A Chemist's View of Binding in Extended Structures* (VCH, New York, 1988).
[5] O. K. Andersen, T. Saha-Dasgupta, R. W. Tank, C. Arcangeli, O. Jepsen, and G. Krier, Lect. Notes Phys. **535**, 3 (2000).
[6] M. Krajčí and J. Hafner, J. Phys.: Condens. Matter **14**, 1865 (2002).
[7] M. Krajčí and J. Hafner, J. Phys.: Condens. Matter **14**, 5755 (2002).
[8] G. B. Bachelet, D. R. Hamann, and M. Schlüter, Phys. Rev. B **26**, 4199 (1982).
[9] D. Vanderbilt, Phys. Rev. B **41**, 7892 (1990).
[10] P. E. Blöchl, Phys. Rev. B **50**, 17953 (1994).
[11] D. Sanchez-Portal, E. Artacho, and J. M. Soler, Solid State Commun. **95**, 685 (1995).
[12] W. C. Lu, C. Z. Wang, T. L. Chan, K. Ruedenberg, and K. M. Ho, Phys. Rev. B **70**, 041101(R) (2004).
[13] T. L. Chan, Y. X. Yao, C. Z. Wang, W. C. Lu, J. Li, X. F. Qian, S. Yip, and K. M. Ho, Phys. Rev. B **76**, 205119 (2007).
[14] X. F. Qian, J. Li, L. Qi, C. Z. Wang, T. L. Chan, Y. X. Yao, K. M. Ho, and S. Yip, Phys. Rev. B **78**, 245112 (2008).
[15] Y. X. Yao, C. Z. Wang, G. P. Zhang, M. Ji, and K. M. Ho, J. Phys.: Condens. Matter **21**, 235501 (2009).
[16] N. Marzari and D. Vanderbilt, Phys. Rev. B **56**, 12847 (1997).
[17] I. Souza, N. Marzari, and D. Vanderbilt, Phys. Rev. B **65**, 035109 (2001).
[18] J. N. Murrell, J. Chem. Phys. **32**, 767 (1960).
[19] J. Ivanic and K. Ruedenberg, Theor. Chem. Acc. **120**, 281 (2008); **120**, 295 (2008).
[20] X. Blase, Lorin X. Benedict, Eric L. Shirley, and Steven G. Louie, Phys. Rev. Lett. **72**, 1878 (1994).